HHS Public Access

Author manuscript

J Comp Neurol. Author manuscript; available in PMC 2022 December 01.

Published in final edited form as:

J Comp Neurol. 2021 December ; 529(17): 3772–3784. doi:10.1002/cne.25193.

A causal role for the pulvinar in coordinating task-independent cortico-cortical interactions

Manoj K. Eradath[1], **Mark A. Pinsk**[1], **Sabine Kastner**[1,2]

[1]Princeton Neuroscience Institute, Princeton University, Princeton, NJ 08544

[2]Department of Psychology, Princeton University, Princeton, NJ 08544

Abstract

The pulvinar is the largest nucleus in the primate thalamus and has topographically organized connections with multiple cortical areas, thereby forming extensive cortico-pulvino-cortical input-output loops. Neurophysiological studies have suggested a role for these transthalamic pathways in regulating information transmission between cortical areas. However, evidence for a *causal* role of the pulvinar in regulating cortico-cortical interactions is sparse and it is not known whether pulvinar's influences on cortical networks are task-dependent or, alternatively, reflect more basic large-scale network properties that maintain functional connectivity across networks regardless of active task demands. In the current study, under passive viewing conditions, we conducted simultaneous electrophysiological recordings from ventral (area V4) and dorsal (LIP) nodes of macaque visual system, while reversibly inactivating the dorsal part of lateral pulvinar (dPL), which shares common anatomical connectivity with V4 and LIP, to probe a causal role of the pulvinar. Our results show a significant reduction in local field potential phase coherence between LIP and V4 in low frequencies (4-15 Hz) following muscimol injection into dPL. At the local level, no significant changes in firing rates or LFP power were observed in LIP or in V4 following dPL inactivation. Synchronization between pulvinar spikes and cortical LFP phase decreased in low frequencies (4-15 Hz) both in LIP and V4, while the low frequency synchronization between LIP spikes and pulvinar phase increased. These results indicate a causal role for pulvinar in synchronizing neural activity between interconnected cortical nodes of a large-scale network, even in the absence of an active task state.

Keywords

Cortico-cortical interactions; Transthalamic pathways; Pulvinar causal role; Reversible-inactivation with muscimol; Macaque Electrophysiology

Corresponding authors Manoj Eradath meradath@princeton.edu, Sabine Kastner skastner@princeton.edu.

Author Contributions

M. K. E and S. K planned and conceptualized the study. M. K. E and M. A. P performed the experiments. M. K. E and M. A. P performed analysis. M. K. E. and S. K. prepared the draft. M. K. E, M. A. P and S. K. reviewed and edited the final draft.

Conflict of interest statement

The authors declare no conflicts of interests

Data sharing

Open toolboxes and custom prepared MATLAB codes were used for analysis. All custom MATLAB scripts and electrophysiological data contained in this manuscript are available upon reasonable request from the corresponding authors Sabine Kastner (skastner@princeton.edu) and Manoj K. Eradath (meradath@princeton.edu)

1. Introduction

The pulvinar is the largest nucleus of the primate thalamus and primarily part of the visual system. It has been implicated in several cognitive functions including orienting to stimuli, filtering of distracter information, and visually guiding motor actions (Robinson & Petersen, 1992, Adams et al., 2000; Shipp, 2003; Kaas & Lyon, 2007; Wilke, 2010). For example, in humans, deficits in filtering distracter information have been observed in patients with pulvinar lesions (Rafal & Posner, 1987; Ward et al., 2002; Arend et al., 2008; Snow et al., 2009), similar to the filtering deficits observed after posterior parietal cortex (PPC) lesions (Posner et al., 1984; Friedman-Hill et al., 2003; Han et al., 2004). In accordance with a role of the pulvinar in attentional processing, monkey physiology studies have shown enhanced responses in subsets of pulvinar neurons following spatial cues that direct attention to a location in the visual field in covert attention tasks (Petersen et al., 1987; Robinson & Petersen, 1992; Saalmann et al., 2012; Zhou et al. 2016; Fiebelkorn et al., 2019a) or in perceptual suppression tasks (Wilke et al., 2009). Deficits in shifting attention to the contra-lesional visual field (Petersen et al., 1987; Desimone et al., 1990) and in performing visually guided movements into the contra-lesional space have been observed as a consequence of pulvinar inactivation (Wilke et al., 2010). Thus, the results from lesion and electrophysiology studies indicate an important role of pulvinar in attentional visuo-spatial processing.

Directly connected cortical areas are generally interconnected via the pulvinar through topographically organized, layer-specific feedforward-feedback connections, forming an extensive network of cortico-thalamo-cortical pathways (Shipp, 2003). Pulvinar subdivisions have been shown to reciprocally connect with the frontal eye field (FEF) (Trojanowski, & Jacobson, 1974; Gutierrez et al., 2000), cingulate and retrosplenial cortex (Watson et al., 1973; Baleydier & Mauguiere, 1985), PPC and extrastriate visual cortex (Yeterian & Pandya, 1985; Adams et al., 2000; Shipp, 2001; Shipp, 2003; Gattass et al., 2014; Arcaro et al., 2015b). It has been suggested that these cortico-thalamo-cortical loops form indirect (transthalamic) pathways through which the pulvinar may influence cortical processing (Kastner & Ungerleider, 2000; Gutierrez et al., 2000; Adams et al., 2000; Shipp, 2001; Shipp, 2003; Gattass, et al., 2014; Arcaro et al., 2015b; Jaramillo et al., 2016; reviewed in Buschman & Kastner, 2015; Fiebelkorn & Kastner, 2020, Kastner et al., 2020). In line with the cortico-thalamo-cortical loop hypothesis, electrophysiological studies have shown that the transthalamic pathways serve to regulate information transmission between interconnected cortical areas (Saalmann et al., 2012; Halassa and Kastner, 2017; Fiebelkorn et al., 2019a, Kaster et al., 2020). Specifically, during selective visual attention, the pulvinar synchronizes neural activity between interconnected cortical areas in the alpha/low beta frequency range (8-15Hz), as shown for visual areas V4 and TEO (Saalmann et al., 2012), the lateral intra parietal area (LIP) and V4 (Saalmann et al., 2018), and LIP and FEF (Fiebelkorn et al., 2019a, Fiebelkorn & Kastner, 2019b). However, it is not clear from these correlational studies whether (i) the pulvinar *causally* influences cortico-cortical interactions and (ii) whether these interactions depend on active task demands.

While inactivation studies of the pulvinar have supported the notion of a causal role for the pulvinar in spatial attention and visually guided motor actions by demonstrating behavioral deficits (Petersen et al., 1987; Desimone et al., 1990; Wilke et al., 2010), only few studies have examined the causal impact of pulvinar inactivation on cortical circuitry by simultaneously recording from cortical areas while selectively altering neural activity in the pulvinar. In anesthetized preparations, it has been shown that focal pharmacological inactivation of the lateral pulvinar significantly reduced evoked visual responses in V1, while focal pharmacological excitation significantly enhanced them (Purushothaman et al., 2012). In awake, behaving monkeys, muscimol inactivation of the ventral portion of the lateral pulvinar caused reduction in attention-related effects in V4 such as decreases in visually-evoked responses and gamma synchrony (Zhou et al., 2016), and, possibly as a consequence of these local effects, reduced functional connectivity between V4 and IT cortex (Zhou et al., 2016). Both the behavioral and electrophysiological effects following pulvinar inactivation suggest a causal influence of the pulvinar on interconnected cortical areas (Zhou et al., 2016; Halassa & Kastner, 2017). However, it is not clear whether the pulvinar influences on cortical areas were active task-related or reflected more basic properties of a large-scale network that maintains functional connectivity regardless of specific task state. Here, we asked whether the pulvinar plays a broader role in regulating functional connectivity across cortical networks by examining the pulvinar's causal influences on interconnected cortical areas under passive viewing conditions. We conducted simultaneous recordings from nodes of the visual system (areas V4 and LIP) while inactivating the dorsal part of the lateral pulvinar (dPL), which shares common connectivity with V4 and LIP, while monkeys passively viewed videos presented on a computer monitor, to explore a causal role of the pulvinar in influencing cortical activity and cortico-cortical interactions in the absence of an active task structure.

2. Materials and Methods

2.1 Animals

Two male macaque monkeys (*Macaca fascicularis*; monkey B and monkey R, age 8 and 14 years, respectively) were used for the study. Princeton University Animal Care and Use Committee approved all surgical and experimental procedures, which conformed with the National Institute of Health guidelines for the humane care and use of laboratory animals.

2.2 Identifying and accessing the interconnected target areas

We performed simultaneous electrophysiological recordings and pharmacological interventions from anatomically and functionally interconnected distant sites. The macaque D99 digital template brain atlas (Reveley et al., 2016) was non-linearly warped to the individual animal's structural MRI images to outline the anatomical locations of the cortical areas of interest and pulvinar subdivisions in the individual animal's anatomical space. The structural connectivity between pulvinar subdivisions and the cortical target areas V4 and LIP was confirmed in one animal with diffusion MR imaging (DMRI). Data were collected for the whole brain on a Siemens 3T MAGNETOM Prisma (80 mT/m @ 200 T/m/s gradient strength) using a 4-channel flexible coil or a surface coil (4-ch Flex Coil Small; 11cm Loop Coil; Siemens AG, Erlangen Germany). Diffusion images were acquired

using a double spin-echo EPI readout pulse sequence with the 4-channel coil wrapped around the head. Two datasets of 270 gradient directions were collected from monkey B using a monopolar gradient diffusion scheme with *b* values distributed optimally across 3 spherical shells (field of view (FOV) = 96mm, matrix size (MS) = 96x96, slice thickness = 1.0mm, in-plane resolution = 1.0 x 1.0mm, slice orientation/order = coronal/interleaved, phase-encode directions = RL LR, number of slices = 50, repetition time (TR) = 6800ms, echo time (TE) = 66ms, phase partial Fourier = 6/8, iPAT = 2 (GRAPPA), fat suppression = on, *b*-values = 850, 1650, 2500 s/mm^3, gradient directions per shell = 90, acquisition time (TA) = 31 min 44 sec). Eighteen non-diffusion weighted images were collected interspersed throughout each dataset. After DMRI pre-processing (de-noising (Veraart et al., 2016; Tournier et al., 2019), Gibbs ringing artifact removal (Perrone et al., 2015; Kellner et al., 2016), susceptibility-, eddy current-, and motion-induced distortion corrections (Andersson et al., 2003), probability distributions of fiber direction at each voxel were derived with FSL (FMRIB, Oxford, UK)'s "Bedpostx GPU" tool (Hernández et al., 2013) considering three fiber populations per voxel (Jbabdi et al., 2012; Behrens et al., 2003; Behrens et al., 2007). These distributions, which take into account fiber direction uncertainty due to MR noise, artifacts, and incomplete modeling of the diffusion data, were used to perform pair-wise mask tractography in order to determine likely fiber pathways between the pulvinar and each cortical area (LIP, V4). Only tracts that passed through the internal capsule were retained. In addition, tracts that entered the opposing hemisphere, the optic nerves, or the external capsule, as well as tracts that extended anterior to the pulvinar were discarded with exclusion masks. Once probable fiber pathways between the pairs were defined, they were thresholded to remove the lower 1% of probable tracts and masked by the pulvinar ROI to delineate cortical projection zones in the pulvinar. We targeted the portion of the lateral pulvinar that showed shared projection zones with LIP and V4 (Figure S1). Averaged high resolution structural scans were used to determine the locations of recording chamber placement and sites for the craniotomies in order to access the brain sites of interest (dorsal portion of lateral pulvinar (dPL), LIP and area V4). Within the chambers, craniotomies of ~4.5 mm size were performed above the areas of interest, while leaving the dura intact. A custom prepared MR-compatible grid tube consisting of a bundle of polyimide tubes was then inserted into each craniotomy to seal the holes, while allowing permanent access to the recording sites. The top of the grid tubes (12-20mm in total length) was then sealed with removable biocompatible silicon adhesives to maintain the aseptic environment. We inserted tungsten micro-electrodes into the cortical areas (LIP and V4) and performed structural MRI scans to verify the electrode locations (Figure S2) by aligning the images with D99 atlas (Saleem & Logethetis, 2007; Reveley et al., 2016).

2.3 Pharmacological inactivation and visualization of the inactivation zone

Muscimol is a γ-aminobutyric acid ($GABA_A$) receptor agonist and its potent central nervous system (CNS) depressant property has been used to reversibly inactivate brain regions of interest. Muscimol rapidly induces a local hyperpolarization around the injected site (Petersen et al., 1987; Majchrzak & Scala, 2000). A custom prepared injectrode assembly (Plastics One Inc, Roanoke, VA) was used to deliver muscimol and to simultaneously record the signals from the lateral pulvinar. The injectrode assembly consisted of 27G fused Silica cannula (od: ~410 μm) with a central core of an epoxy coated tungsten electrode

(~125 μm). The cannula was positioned based on the measurements from the structural and diffusion MR images. We used Gadolinium, an MRI contrast agent (Magnevist, 5mM solution), to visualize (i) the initial injection site and (ii) approximate the time course of the spreading of the agent around the initial site of injection. At the beginning of each session, the monkey was sedated with a combination of ketamine (5mg/Kg) and xylazine (1mg/Kg), and the injectrode was inserted into the dPL through the grid tube. An MR scan was acquired to confirm the initial position of the injectrode by visualizing its tip. Then, 0.5 μl of Gadolinium was pressure delivered through the injectrode using a gas-tight Hamilton syringe (10μl capacity) at a rate of 0.05μl/min with the help of an automated drug delivery pump (Harvard Apparatus, MA). The macaque D99 digital template brain atlas was non-linearly warped to the animal's MR images to confirm the initial site of the Gadolinium contrast agent injection within the dorsal portion of the lateral pulvinar (Figure 1A). After the animals recovered from the sedation, they were taken to the experimental setup for electrophysiological recordings. 1μl of muscimol solution in sterile Phosphate buffered Saline (PBS) with an effective muscimol concentration of 6.67μg/μl or 1μl of sterile PBS was pressure delivered through the injectrode during the inactivation and control sessions, respectively. We performed 12 muscimol inactivation sessions (8 in monkey B and 4 in monkey R) and 10 saline control sessions (7 in monkey B and 3 in monkey R). In monkey B, we also tracked the spread of the contrast agent from the initial point of contrast injection with the help of multiple repeated structural scans over a period of 3 hours after an injection of 1.0μl of Gadolinium contrast agent into dPL. 10 T1-weighted volumes were collected (at times 0, 15, 30, 45, 60, 75, 90, 105, 120, and 180 minutes from the end of injection), with the surface coil secured above the head to obtain high-quality structural volumes (3D magnetized prepared rapid gradient echo (MPRAGE) sequence; FOV = 128mm, MS = 256x256, slice thickness = 0.5mm, in-plane resolution = 0.5 x 0.5mm, slice orientation/order = sagittal/interleaved, TR = 2700ms, TE = 2.32ms, inversion time = 850ms, flip angle = 9 deg, number of slices = 240, TA = 11 min 21 sec). These data provided an approximation of the spread of injected substance over the course of a recording session (Figure 1B). Based on the data of the temporal spread of the Gadolinium contrast agent within the pulvinar, two windows of interests were identified. A 15-minute window immediately before the start of injection (muscimol or PBS control) was used as pre-injection baseline window while a 15-minute window starting from 15 minutes after the end of injection (indicated by orange bar in Figure 1B) as the post-injection window. The spread of gadolinium contrast agent was approximately within the anatomical boundaries of dPL (a volume $3mm^3$) during this 15-minute post-injection window (15-30 minutes from the end of injection). Depending on the site of injection, previous studies have reported behavioral effects of muscimol inactivation to last more than 12 hours, but behavior returning to a normal baseline within 24 hours (Wilke et al., 2010). We took specific precautions to avoid residual drug effects on subsequent sessions by separating the muscimol and saline control recording sessions in pulvinar by a minimum of 48 hours, thereby minimizing residual effects of muscimol, particularly on control sessions.

2.4 Electrophysiology

Epoxy coated single unit tungsten microelectrodes (FHC Inc.) were used in monkey B, while 32 channel multi-contact probes (V-probe, Plexon Inc., Dallas, TX) were used in

monkey R for recordings of spiking activity and local field potentials (LFP). The electrodes were lowered at different angles and locations to each of the cortical areas using independent microdrives (NAN instruments). Electrophysiology signals were collected at a sampling rate of 40,000Hz for spikes and 1,000 Hz for LFPs, using a head-stage amplifier and recording system (Plexon Inc., Dallas, TX). A skull screw inserted over the opposite hemisphere (over primary motor cortex, AP +17, distance in mm from ear bar zero) and outside of the recording chambers was used as a reference for electrophysiological recordings. Inactivation/electrophysiological sessions were performed only after a minimum of 2 hours following the last ketamine/xylazine injection, after animals completely recovered from sedation. At the beginning of the session, the animals performed a receptive field (RF) mapping task to position the electrodes, so that RFs matched across the three areas. An infrared eye tracker (EyeLink, 1000 Plus, SR Research Ltd, Ottawa, CAN) was used to monitor the animal's eye positions during the RF mapping task. RF mappings were done online by flashing bright discs of 2-degree visual angle in 8 quadrants of the screen while animals maintained fixation at a central a fixation square (0.5°). The neural responses evoked by the stimuli were then analyzed online (Neuroexplorer, Plexon Inc., Dallas, TX) to identify the RFs of the recorded locations. Specifically, high-gamma (70-150Hz) power was calculated for each of the 8 locations over a minimum of 10 trials for each location. The maximum response across the 8 locations was calculated and if the maximum response exceeded 60% of the mean response across all locations, the response was considered as significant, and the location corresponding to the maximum response was regarded as the RF of the particular cell/channel. RFs were considered overlapping between cells/channels if exhibiting significant responses (by the above definition) in the same location. The mappings were done online at the time of electrode placement and the electrode positions were adjusted until matching RFs were obtained across all 3 recorded areas (dPL, LIP and V4). At the end of each recording session, RF mappings were repeated to ensure the stability of RFs and to identify cells/channels with mismatched RFs, which were then excluded from further analysis. Spiking activity and LFPs were recorded simultaneously from dPL, LIP and V4 in monkey B and from LIP and V4 in monkey R. During the inactivation and electrophysiological recordings, the animals remained in a primate chair, head fixed, while freely viewing a video (short clips of documentary 'snow monkeys', PBS nature documentary), presented on the LCD monitor, placed in front of the chair. The same video clips were played during all recording sessions and for both animals. In order to assess any visual field deficits as a consequence of pulvinar inactivation/injection, monkeys performed a visually guided saccade task at the end of the session. In this task, the animals directed their gaze to and maintained fixation for 500ms at spatial cues, presented sequentially in different locations of the visual field. The animals did not show visual field deficits following inactivation/injection of dPL according to this test. Simultaneous LIP and V4 recordings were performed in both animals, while additional simultaneous pulvinar recordings during injection sessions were obtained only from monkey B (n=8, muscimol sessions, n=7, saline control sessions).

2.5 Data analysis

LFP power and spike rates: Powerline noise was removed from the LFP signals using a Butterworth notch filter (filter designed using the *designfilt* function of MATLAB with

notch defined as the 59 to 61 Hz frequency interval). The Hilbert transform was then applied to the LFP data to obtain instantaneous power over a frequency range of 4- 90 Hz. The percentage change in LFP power was calculated by comparing the 15 minutes post-injection window with that of the 15-minutes pre-injection window. The percentage changes between muscimol and control sessions were statistically compared using the Wilcoxon rank-sum test. Spiking activity was processed offline (Offline sorter, Plexon, Inc., Dallas, TX) to identify spike waveforms that crossed the threshold over 4 standard deviations from the mean of peak heights in the histogram. The single-unit/multi-unit (SUA/MUA) clusters were isolated by running a valley seeking algorithm, which assigned the waveforms into optimal number of clusters based on the inter-point distances in the feature space (Offline sorter, Plexon, Inc., Dallas, TX). A total of 56 LIP cells (monkey B: 20 cells, monkey R: 36 cells) and 50 V4 cells (monkey B: 10 cells, monkey R: 40 cells) were recorded during the muscimol inactivation sessions. 37 LIP cells (monkey B: 10 cells, monkey R: 27 cells) and 31 V4 cells (monkey B: 8 cells, monkey R: 23 cells) were recorded during the saline control sessions. Additionally, in monkey B, pulvinar neurons were recorded during the sessions (8 cells in muscimol sessions and 7 cells in control sessions).

Coherence analysis: Estimation of frequency domain coherence is a useful tool for analyzing interactions between simultaneously recorded neural signals. Here, we used two different coherence measures to explore the interactions between cortical areas during pre- and post- injection time windows. Phase locking value (PLV) is a metric used for quantification of frequency-specific synchronization between LFP signals recorded from different brain areas (Lachaux et al., 1999) and is assumed to be a measure of inter-areal functional connectivity. PLV uses only the phase values to calculate the coherence between two simultaneously recorded signals. The Hilbert transform was used to determine instantaneous phase of LFP data binned into 1-second time segments over a frequency range of 4-60 Hz. Instantaneous I phase was then used to calculate PLV, as defined by the equation $PLV(t) = \frac{1}{N} \left| \sum_{n=1}^{N} e^{i\theta(t,n)} \right|$, where N is the total number of time bins of LFP data and $\theta(t,n)$ is the difference between the instantaneous phase of two signals at time t and time bin n, in a given frequency band. The resulting PLV for each frequency was averaged over 1-second time segments to obtain frequency specific interareal PLV. The Wilcoxon sign-rank test was used to statistically compare the PLV obtained pre- and post-injection, and in muscimol and control sessions. We further confirmed the inter-areal coherence by computing LFP-LFP spectral coherence from pairs of multi-taper estimate of spectra of LFP-LFP pairs, over a frequency range of 4-60Hz, from LFP data binned into 1-second time segments (*coherencyc* script from Chronux toolbox, Chronux.org). The Wilcoxon sign-rank test was used to statistically compare the LFP-LFP coherence measures obtained during pre- and post-injection, and in muscimol and control sessions. While PLV and LFP-LFP spectral coherence analyses provide measures of inter-areal synchronization, it does not inform about the directionality of the interaction. For that purpose, we computed spike-field coherence (SFC), which measures the clustering of spiking activity in one area relative to specific phases of simultaneously recorded frequency-specific LFP signals from a second area, and thereby provides an alternative estimate of network connectivity between regions (Fries et al., 2001). Since spiking activity is generally considered to be an area's output signal and LFP activity an area's input signal, SFC provides indirect evidence for the

directionality of inter-areal interactions (Pesaran, 2010). SFC between pulvinar and cortical areas was calculated over a frequency range of 4-60Hz, from LFP and spike data binned into 1-second time segments (*coherencycpt* script, Chronux toolbox, Chronux.org). Changes in SFC between pulvinar and cortical areas during pre- and post-injection were calculated in both directions (i.e. pulvinar spike to LIP phase, LIP spike to pulvinar phase, pulvinar spike to V4 phase, and V4 spike to pulvinar phase). The Wilcoxon rank-sum test was used to statistically compare the changes in SFC values calculated separately for muscimol and control sessions. Coherency measures are known to be positively biased towards smaller sample sizes of spikes or trials (Vinck et al., 2010). To address this issue, we conducted a control analysis and computed Pairwise Phase Consistency (PPC) as an alternative method for estimating spike field coherence. This method has been reported to be a bias-free coherence measure (Vinck et al., 2010). PPC measures avoid the sample number bias in the coherence estimations by replacing the vector addition step (of SFC calculation) by vector dot product of pairs of relative phases. Changes in PPC between pulvinar and cortical areas during pre- and post-injection were calculated ('ppc0' script of Fieldtrip Toolbox, https://www.fieldtriptoolbox.org/) in both directions from LFP and spike data binned into 1-second time segments over a frequency range of 4-60Hz.

3. Results

We performed simultaneous recordings of spiking activity and LFPs from areas LIP and V4 of awake, head-fixed monkeys while freely viewing short video clips presented on a LCD screen placed in front of the primate chair (see methods for details), before and after inactivating the dorsolateral pulvinar (dPL) by injecting the $GABA_A$ agonist muscimol, or by injecting saline as a control. Based on previous studies that showed robust functional connectivity of interconnected large-scale networks even in the absence of active task requirements (Wang, 2012; Arcaro, 2015a), we used simultaneous electrophysiological recordings under passive viewing condition to probe the causal role of pulvinar in coordinating interactions across cortical networks.

3.1 Local responses in cortical areas and pulvinar following muscimol inactivation

First, we examined local effects of muscimol inactivation on firing rates and LFP power in cortical areas LIP and V4. Firing rates in LIP did not significantly change following muscimol (pre-injection: 11.51 ± 1.15 Hz; post-injection: 11.94 ± 1.17 Hz, mean ± s.e.m., n=56; p=0.70, Wilcoxon sign-rank test) or control (pre-injection: 9.39 ± 0.67 Hz; post-injection: 10.77 ± 0.66 Hz, mean ± s.e.m., n=37; p=0.13, Wilcoxon sign-rank test) injections (Figure 2A, left). LFP power in LIP before and after the injections was also not significantly different between muscimol and saline control sessions in any of the frequency ranges that were examined (theta (4-7 Hz) p= 0.97; alpha/low-beta (7-15 Hz) p= 0.53; beta (15-30 Hz) p=0.49; low-gamma (30-60 Hz) p=0.28; or high-gamma (60-90 Hz) p= 0.93, Wilcoxon rank-sum test) (Figure 2A, right). Similarly, V4 firing rates did not significantly change following muscimol (pre-injection: 24.30 ± 3.41 Hz; post-injection: 25.09 ± 3.32 Hz, mean ± s.e.m., n=50; p=0.32, Wilcoxon sign-rank test) or control (pre-injection: 26.71 ± 4.89 Hz; post-injection: 31.55 ± 5.27 Hz, mean ± s.e.m., n=31; p=0.20, Wilcoxon sign-rank test) injections into dPL (Figure 2B, left). Also, LFP power in V4 was not significantly different

between muscimol and control sessions in any of the frequency bands tested (theta (4-7 Hz), p= 0.44; alpha/low-beta (7-15 Hz), p=0.92; beta (15-30 Hz), p= 0.97; low-gamma (30-60 Hz), p=0.82; high-gamma (60-90 Hz), p=0.82; Wilcoxon rank-sum test) (Figure 2B, right). In monkey B, we also recorded spiking activity and LFPs from dPL in addition to LIP and V4 before and after injections with muscimol, or saline, respectively. Baseline firing rates of neurons in dPL were significantly reduced following muscimol injections (pre-injection: 10.69 ± 1.76 Hz; post-injection: 5.48 ± 1.06 Hz, mean ± s.e.m., n=8; p=0.04, Wilcoxon sign-rank test) but not after control injections (pre-injection: 4.33 ± 0.36 Hz; post-injection: 4.46 ± 0.29 Hz, mean ± s.e.m., n=7; p=0.81, Wilcoxon sign-rank test). The mean baseline firing rate during saline control sessions (4.33 ± 0.36 Hz) was lower as compared to the mean baseline rate during muscimol sessions (10.69 ± 1.76 Hz) in pulvinar, which could be attributed, in principle, to residual long-term muscimol effects. However, we do not think that the lower baseline firing rates during saline sessions as compared to muscimol sessions can be attributed to residual muscimol effects on the control sessions, given that we separated muscimol and saline sessions by a minimum of 48 hours and intermingled both types of sessions. We also examined high gamma activity (HGA, 60-90Hz), which is often interpreted as a surrogate for mulit-unit activity (Ray et al., 2008; Ray & Maunsell, 2011; Watson et al., 2018). Consistent with the reduction in spike rates, the power of HGA in dPL was significantly reduced, following muscimol injections compared to control sessions (p=0.04, Wilcoxon rank-sum test, 8 muscimol sessions, 7 control sessions). No significant changes in LFP power were observed in other frequency bands tested (theta (4-7 Hz), p=0.46, alpha/low-beta (7-15 Hz), p=0.78, beta (15-30 Hz), p=0.96, low gamma (30-60 Hz), p=0.39, Wilcoxon rank-sum test) during muscimol inactivation sessions relative to saline control sessions (Figure S3). Taken together, the present results show significant reduction of firing rates and high gamma (60-90Hz) LFP power locally following muscimol injections into dPL, confirming the suggested role of GABAergic neurons in controlling the excitability of local thalamic neuronal populations (McCormick & Prince 1987). However, no remote effects on neural activity in the two interconnected cortical areas were found with respect to baseline firing or LFP power changes as a consequence of dPL inactivation, suggesting that dPL inputs are not critical in maintaining the task independent baseline firing and LFP activity within LIP and V4.

3.2 Effects of pulvinar inactivation on cortico-cortical connectivity

Next, we explored the functional role of the pulvinar on cortico-cortical connectivity by measuring the phase locking value (PLV) between cortical areas LIP and V4, pre- and post-muscimol or control injections into dPL. PLV is a measure of LFP phase coherence between areas and is thought to be an effective index for quantifying interareal synchronization, or functional connectivity (Lachaux et al., 1999). During inactivation sessions, the LFP-LFP phase coherence between LIP and V4 was significantly reduced in theta (4-7 Hz) and alpha/low-beta (7-15 Hz) frequency bands following muscimol injections compared to pre-injection phase coherence values (theta: p=0.04, alpha/low-beta: p=0.002, n=12 sessions, Wilcoxon sign-rank test). The LFP-LFP phase coherence was not significantly different during the muscimol sessions in any other frequency bands tested (beta (15-30Hz): p=0.08 and gamma (30-60 Hz): p=0.13, n=12 sessions, Wilcoxon sign-rank test) (Figure 3, left). The frequency band-specific decrease in phase coherence values was present in both animals

(monkey B: alpha/low-beta: p=0.03, p > 0.05 in all other frequency bands tested, n=8 sessions, Wilcoxon sign-rank test, monkey R: theta: p=0.04, alpha/low-beta: p=0.05, p > 0.05 in all other frequency bands tested, n=4 sessions, Wilcoxon sign-rank test, one sided). In control sessions, the LIP-V4 phase coherence was not significantly different between pre- and post-control injection sessions in any of the frequency bands tested in combined data from both animals (theta: p=0.73; alpha: p=0.82; beta: p=0.43; gamma: p=0.25, n=10 sessions, Wilcoxon sign-rank test) (Figure 3, right), or in individual animals (monkey B: p >0.05 in all frequency bands tested, n=7 sessions, monkey R: p > 0.10, in all frequency bands tested, n=3 sessions, Wilcoxon sign-rank test). The frequency specific LIP-V4 phase coherence decrease following the muscimol injection into dPL was persistent within the time windows used for analysis (Figure S4). Consistent with these results, an alternative measure of functional connectivity, LFP-LFP spectral coherence between LIP and V4, yielded significant coherence decrease in theta (4-7 Hz), alpha/low-beta (7-15 Hz) and beta (15-30 Hz) frequency bands following muscimol injections (p=0.034, p=0.007 and p=0.043 respectively, n=12 sessions, Wilcoxon sign-rank test). The LIP-V4 spectral coherence was not significantly different in gamma frequency band (p > 0.1, Wilcoxon sign-rank test) (Figure S5, left). No significant differences between pre-and post-injection LIP-V4 spectral coherence were observed following control injections (p > 0.1, Wilcoxon sign-rank test, in all four frequency bands) (Figure S5, right). Previous studies have suggested, based on correlational analyses, that the pulvinar regulates information processing between interconnected cortical areas depending on task demands in a spatial attention task by modulating functional connectivity in alpha-low beta (8-15 Hz) frequency bands (Saalmann et al., 2012; Fiebelkorn et al., 2019a). However, causal evidence for such a role of pulvinar in cortico-cortical synchronization has been lacking. Here, we show that the pulvinar appears to regulate functional connectivity across interconnected areas in low frequency (4-15 Hz) bands, even in the absence of active task conditions.

3.3 Changes in pulvino-cortical connectivity following pulvinar inactivation

Thus far, our results show that pulvinar inactivation caused a significant reduction in cortico-cortical interactions between LIP and V4 even in the absence of an active task state, while not significantly changing the neuronal firing or LFP power in LIP and V4. In monkey B, we tested the effect of pulvinar inactivation on the phase coherence between pulvinar and cortical areas. Both the pulvinar-LIP and pulvinar-V4 phase coherence values were marginally reduced in alpha/low-beta (7-15 Hz) frequency bands following the muscimol injections into dPL (pulvinar-LIP, p=0.05, (Figure S6 A, left); pulvinar-V4, p=0.06, (Figure S6 B, left), p > 0.05 in all other frequency bands tested, n=8 sessions, Wilcoxon sign-rank test), but not after the control injections (p > 0.05, in all frequency bands tested, both for pulvinar-LIP and pulvinar-V4 coherences, n=7 sessions, Wilcoxon sign-rank test) (Figure S6 A, B, right). These results confirm that the pulvino-cortical connectivity that is mediated through neuronal synchronization in the alpha/low beta frequencies observed during attention tasks is present even in the absence of an active task state. However, the LFP-LFP phase synchronization is not informative regarding the direction of the observed inter-areal interaction.

Therefore, we measured spike field coherence (SFC) between pulvinar and cortical areas to further explore pulvino-cortical interactions. SFC is an indirect measure of the relationship between spiking outputs from one region to the synaptic inputs (LFP) of a second region, and thus provides a useful measure for exploring inter-areal input-output interactions (Fries et al., 2001; Pesaran, 2010). A frequency-specific increase in SFC can be interpreted as arising from the area that produces spiking output and being directed at LFP signals of the input area (Pesaran, 2010). We measured SFC between pulvinar and cortical areas in both directions (from pulvinar to cortex and from cortex to pulvinar), for pre- and post-injection windows. SFC between pulvinar spiking activity and LIP LFP phase post- vs. pre-injection was significantly lower after muscimol injection in theta-alpha/low-beta (4-15 Hz) frequencies, as compared to the corresponding difference after control injections ($p=0.01$, $p > 0.05$ in beta and gamma frequency ranges, Wilcoxon rank-sum test) (Figure 4A, left). Similarly, the difference in SFC between pulvinar spikes and V4 LFP phase was significantly reduced in theta-alpha/low-beta frequencies after dPL inactivation compared to corresponding measures after control sessions ($p=0.03$, $p > 0.05$ in beta and gamma frequency ranges, Wilcoxon rank-sum test) (Figure 4B, left). Interestingly, the difference in SFC between LIP spikes and pulvinar LFP phase significantly increased in a similar theta-alpha/low-beta frequency range following the muscimol injections into dPL, as compared to control injections into dPL ($p=0.02$, $p > 0.05$ in beta and gamma frequency ranges, Wilcoxon rank-sum test) (Figure 4A, right), indicating an increase in spike-field coherence between LIP spikes and pulvinar phase following the muscimol injections into dPL. No such increase in SFC was observed between V4 spikes and pulvinar LFP phase in this or any other frequencies (theta-alpha/low-beta: $p=0.69$; other frequencies: $p> 0.05$; Wilcoxon rank-sum test) (Figure 4B, right). Since the spike field measures provide indirect evidence for the directionality of inter-areal influences (i.e. spikes as output signals from an area and LFPs input signals into an area), the current SFC results suggest a significant decrease in network connectivity from pulvinar to cortical areas (LIP and V4) in low frequencies (4-15Hz), following the muscimol inactivation of dPL. Our results also suggest that the network connectivity from LIP to pulvinar, but not from V4 to pulvinar, is significantly increased following dPL inactivation.

SFC measures are known to be positively biased towards smaller sample sizes of spikes or trials (Vinck et al., 2010). To rule out that our SFC measures were influenced by such biases, we conducted a control analysis by computing Pairwise Phase Consistency (PPC), a bias-free coherence measure (Vinck et al., 2010) for estimating spike field coherence. Similar to the results shown in Figure 4, PPC measures also showed a decrease in low frequency coherence between pulvinar spikes and cortical LFPs while the coherence between LIP spikes and pulvinar LFP increased, following the muscimol injections (Figure S7), thereby confirming our previous results using an alternative method. Taken together, these results are consistent with and complement our main finding that pulvinar inactivation interferes with cortico-cortical interactions mediated in low frequencies (4-15Hz).

4. Discussion

We performed simultaneous recordings from dorsal (LIP) and ventral (V4) areas of the visual system, while reversibly inactivating their anatomically interconnected subdivision

of the pulvinar (dPL) in monkeys during passive viewing conditions. The results show a significant reduction in phase coherence of local field potentials (LFP) between LIP and V4 in low frequencies (4-15 Hz) following muscimol injection into dPL. This finding provides causal evidence for a role of the pulvinar in regulating cortico-cortical functional connectivity even in the absence of an active task state. Our results suggest that the pulvinar's influence on cortico-cortical interactions is not limited to specific task requirements, as previously shown (Saalmann et al., 2012), but is part of more basic functional connectivity that is maintained during resting states and can be modulated by task demands. At the local level, no significant changes in firing rates or LFP power were observed in LIP or in V4 following dPL inactivation, indicating that dPL inputs were not critical in maintaining local response properties within extrastriate, or parietal visual areas under these conditions. However, significant decreases in synchronization between pulvinar spikes and cortical LFP phase were observed both in LIP and V4, following dPL inactivation. The reduction in pulvino-cortical spike field coherence was specific for theta-alpha/low-beta frequencies (4-15Hz), suggesting a role for pulvinar spike inputs in frequency-specific synchronization of cortico-cortical interactions.

Electrophysiological studies on the pulvinar have provided evidence for a role in regulating information transmission between ventral visual areas (Saalmann et al., 2012; Zhou et al., 2016), or between higher-order cortical areas (e.g. FEF and LIP as shown in Fiebelkorn et al., 2019a) during spatial attention tasks. These studies have explored the role of pulvinar under specific task conditions, leaving open the question as to whether the pulvinar influences on cortico-cortical functional connectivity are related to engagement in specific tasks, or rather a more basic property of large-scale network connectivity that is maintained regardless of specific task conditions. Studies in humans have suggested functional connectivity between pulvinar and cortical areas even in the absence of any active task structure, based on BOLD responses (Stein et al., 2000; Barron et al., 2015; Arcaro et al., 2015b; Terpou et al., 2018). Watching short movie clips during data collection provides a way to keep subjects engaged and has been shown to be a reliable method for obtaining functional connectivity data both in monkeys (Mantini et al., 2013) and in humans (Vanderwal et al., 2015; Vanderwal et al., 2019). In the current study, we adopted this method and recordings were performed while animals freely viewed short movie clips.

Muscimol, a $GABA_A$ agonist which causes local hyperpolarization, has been extensively used to reversibly inactivate brain regions and to explore causal relationships (Petersen et al., 1987; Desimone et al., 1990; Wilke et al., 2010; Purushothaman et al., 2012; Zhou et al., 2016). Previous inactivation studies probing a causal role for the pulvinar in influencing local cortical responses have shown various effects on baseline, visually evoked, or task-related responses. In anesthetized preparations, both baseline firing rates and visually-evoked responses were found to be significantly reduced in V1 following muscimol injections into the lateral pulvinar (Purushothaman et al., 2012). In contrast to V1 responses in anesthetized recordings, baseline firing rates in V4 neurons were only marginally increased in awake monkeys performing an attention task, following muscimol injections into the ventro-lateral pulvinar (Zhou et al., 2016). Visually evoked responses, however, were significantly decreased following ventro-lateral pulvinar inactivation (Zhou et al., 2016), suggesting that pulvinar influences are critical to enable cortical information

processing (see Fiebelkorn & Kastner, 2020; Kastner et al., 2020 for review). In the current study, we did not find any significant changes in task-independent baseline firing rates or LFP power following muscimol injection into dPL. It is possible that the differences in preparation (anesthetized vs. awake behaving) account for the differences in pulvinar inactivation effects on baseline firing rates between V1 and V4, as observed in these studies. However, alternatively, it is possible that there is a fundamental difference between pulvino-cortical loops involving primary visual versus extrastriate cortex, as suggested by studies in rodent somatosensory cortex (Sherman, 2007; Theyel et al., 2009). This possibility remains to be probed in future studies in primates. Taken together, the effects of pulvinar inactivation on baseline firing rates, observed previously (Zhou et al., 2016) and in the present study suggest that pulvinar inputs do not appear to impact local neuronal response properties in the absence of active task demands in extrastriate area V4 and in parietal area LIP.

Immunohistochemistry experiments in the past have shown the distribution of GABAergic neurons across different mammalian thalamic structures (Sivilotti & Nistri, 1991; Arcelli et al., 1997). For the pulvinar, moderate to high densities of GABAergic neurons were observed in lateral, medial and inferior subdivisions of the pulvinar in monkeys (Hunt et al., 1991; Huntsman et al., 1996). These studies have suggested a crucial role for GABAergic neurons in regulating thalamocortical circuits by changing the excitability of local thalamic populations (McCormik & Prince, 1987; Tremblay et al., 2016). $GABA_A$ mediated mechanisms (i.e. inhibitory-inhibitory (I-I) and excitatory- inhibitory (E-I) models) have been proposed to underlie the generation of gamma oscillations in cortex (Whittington et al., 2000; Cardin et al., 2009; Buszaki & Wang, 2012). Our results showed a significant decrease in gamma power following $GABA_A$ agonist injections into dPL, suggesting that gamma activity in the pulvinar may depend on $GABA_A$ mechanisms, like those observed in cortex.

The distribution of different GABA receptor subtypes ($GABA_A$, $GABA_B$ and $GABA_C$) varies between species/nuclei. For example, the LP nucleus of rats shows a higher density of $GABA_B$ receptors (Bowery et al., 1987). In rhesus monkeys, the highest level of $GABA_B$ receptors has been noted in the latero-posterior pulvinar complex (Bowery et al., 1999; Neto et al., 2006). Different GABA receptor subtypes differ in their ligand binding dynamics and electrophysiological properties. Recent computational models suggest that each may have distinct roles in thalamic function. $GABA_B$ appears to preferentially regulate spontaneous activity, while $GABA_A$ may preferentially mediate evoked activity (Park et al., 2014). Given that muscimol is a potent and selective agonist to $GABA_A$ receptors, its effect in reducing, but not eliminating spontaneous firing rates in pulvinar suggests that other GABA receptor subtypes contribute to the regulation of spontaneous activity (also in agreement with the model proposed by Park et al., 2014). For example, a combination of muscimol (selective $GABA_A$ agonist) and Baclofen (selective $GABA_B$ agonist) may result in a greater reduction or even elimination of spontaneous firing in pulvinar.

In-vitro and in-vivo studies in cat LGN have shown that alpha and theta oscillations can be glutamatergically (Hughes et al., 2004) or cholinergically (Lorincz et al., 2008) induced by activating a subset of thalamocortical (TC) neurons, so called high threshold burst firing (HT) neurons. These Ca2+-dependent neurons burst at frequencies of about 10Hz and

generate synchronized oscillations with the help of gap junctions, that is via electrical, not neurochemical coupling (Hughes et al., 2004; Hughes & Crunelli, 2005). Slice studies have shown that particularly cholinergically induced alpha oscillations were resistant to blocking glutamate or $GABA_{A/B}$ receptors, but were abolished using gap junction blockers (Lorincz et al., 2008). Our results showed no significant decrease in theta or alpha power in the pulvinar following muscimol – a $GABA_A$ agonist – injections. This result suggests that the generation of these oscillations may depend on non-GABA mediated mechanisms, and it is possible that similar non-GABA mediated alpha and theta generators are at play in the primate pulvinar as shown for the cat LGN. Future pharmacological studies will be needed to explore the specific mechanisms underlying the generation of slow frequency oscillations in the primate pulvinar.

In addition to local interneurons, thalamo-cortical neurons in pulvinar receive inhibitory input from the thalamic reticular nucleus (TRN). TRN is constituted of a thin layer of exclusively GABAergic inhibitory neurons, covering the lateral and anterior aspects of dorsal thalamus. The collateral branches of cortico-thalamic axons provide unidirectional glutamatergic excitatory inputs to TRN while the connectivity of TRN with thalamus is bidirectional, with collateral branches of thalamocortical axons providing excitatory inputs and TRN providing inhibitory inputs back to the thalamus, in a closed (reciprocal connections between the same TRN and thalamus regions) or in an open (input from one region of thalamus and TRN output to another region of thalamus or to local inhibitory interneurons) loop manner (Pinault, 2004; Zikopoulos & Barbas, 2007; Gattass et al., 2014). Electrophysiological studies have shown modality-specific sectors within TRN, each connected to different thalamic nuclei and associated cortical areas (Pinault, 2004; Crabtree, 2018). Glutamatergic driver inputs from thalamocortical and corticothalamic axonal collaterals to TRN constitute an important feedback loop for the thalamus-TRN-thalamus network. GABAergic inhibition of thalamus can influence thalamic responses to cortical inputs and thereby affecting feedback responses from thalamus to TRN, which in turn affects modulatory influences of TRN on thalamus (John et al., 2018). Functional interactions within the cortico-TRN-thalamus network have been shown to be modulated by cognitive tasks (McAlonan et al., 2008; Halassa, et al., 2014; Wimmer et al., 2015). While the findings of deafferented TRN generating alpha-low beta spindle rhythms (Steriade et al., 1987) indicate a possible pacemaker role of TRN in thalamic alpha-low beta rhythms, the reciprocal inputs from thalamus to TRN may be important in sustaining and resetting the phase of these rhythms (Saalmann et al., 2011). In this context, muscimol inactivation may disrupt such phase resetting of thalamic oscillations, and GABAergic inhibition of thalamus may prevent rebound excitation from thalamic cells to TRN, leading to alpha-low beta oscillations that are decorrelated from cortical inputs (John et al., 2018).

Previous studies suggest that the pulvinar coordinates information transmission across cortical areas by synchronizing their activity in alpha/low beta frequencies (Saalmann et al., 2012). For example, during a spatial attention task, the LFP-LFP coherence between V4 and TEO, as well as between V4 and the pulvinar and between TEO and the pulvinar, respectively, was significantly increased when attention was deployed at a RF as compared to away from it, predominantly in alpha/low-beta (8-15 Hz) frequencies. Granger analysis suggested a causal influence from pulvinar to cortex (Saalmann et al.,

2012). Here, we provide critical empirical evidence for this notion by perturbing the V4-LIP-dPL network with an actual causal manipulation and by demonstrating a decrease in neural synchronization between V4 and LIP in a similar frequency band following muscimol inactivation of the interconnected dPL. Thus, perturbation of the pulvinar appears to affect primarily the functional connectivity of interconnected network nodes (Figure 5B), substantiating the notion that pulvinar plays a causal role in coordinating inter-areal functional interactions in cortex.

Recent studies performing simultaneous recordings from pulvinar and cortical nodes of the fronto-parietal attention network (FEF and LIP) have further established a role of the pulvinar in regulating cortico-cortical interactions in spatial attention tasks (Fiebelkorn et al., 2019a). It was shown that the medial pulvinar rhythmically engaged and disengaged with the cortical nodes (FEF and LIP) during the allocation of attention in alpha/low beta (14 -24 Hz) frequencies. During periods of attentional engagement, Granger analyses suggested that information flowed from the pulvinar to cortex via the transthalamic pathway, thereby facilitating visual processing. The direction reversed from cortex to the pulvinar during periods of attentional disengagement, suggesting a suppression of visual information across the transthalamic pathway (Fiebelkorn et al., 2019a, Fiebelkorn & Kastner, 2019b; Figure 5A). Computational studies have proposed that cholinergically induced alpha from the thalamus to cortex is related to facilitating visual information processing in cortex, while glutamatergically induced alpha from layer 5 neurons in cortex (Silva et al., 1991) may suppress this function (Vijayan & Kopell, 2012). In the current study, we found a significant decrease in spike-field coherence between pulvinar spikes and LFP phases in V4 and LIP following muscimol inactivation specifically in low frequency (4-15 Hz) ranges. Interestingly, the spike-field coherence between LIP spikes and pulvinar phase was found to be increased following pulvinar inactivation in similar frequency ranges (Figure 5). With the general notion of spikes being output signals and LFPs being input signals (Pesaran, 2010), the current SFC findings suggest that neural activity in low frequencies of the LFP from cortex to the pulvinar dominated following pulvinar inactivation, setting up functional interactions between pulvinar and LIP, similar to those observed during states of attentional disengagement in recent studies (Fiebelkorn et al., 2019a; Fiebelkorn & Kastner, 2019b). These dominating cortical influences on the pulvinar during inactivation may prevent the transthalamic pathway from executing its gating function to set up effective functional interactions between cortical areas.

In summary, our results reveal a causal role of pulvinar in regulating cortico-cortical interactions even in the absence of an active task structure. The results suggest that pulvinar inputs may not impact baseline responses, at least in extrastriate cortex, but rather are critical in synchronizing responses between different interconnected cortical nodes of a cortical large-scale network. Future studies of pulvinar inactivation and simultaneous recordings from nodes of the fronto-parietal network under behavioral tasks will be necessary to further establish causal mechanisms of task-dependent selective cortical engagement by the pulvinar during attention and other cognitive tasks.

Supplementary Material

Refer to Web version on PubMed Central for supplementary material.

Acknowledgments

This work was supported by grants from NEI (2R01EY017699) and NIMH (2R01MH064043, P50MH109429).

References

Adams MM, Hof PR, Gattass R, Webster MJ, & Ungerleider LG (2000). Visual cortical projections and chemoarchitecture of macaque monkey pulvinar. Journal of Comparative Neurology, 419, 377–393.

Andersson JLR, Skare S, & Ashburner J (2003). How to correct susceptibility distortions in spin-echo echo-planar images: application to diffusion tensor imaging. NeuroImage, 20, 870–888. [PubMed: 14568458]

Arcaro MJ, Honey CJ, Mruczek REB, Kastner S, & Hasson U (2015a). Widespread correlation patterns of fMRI signal across visual cortex reflect eccentricity organization. Elife, 2015, 1–28.

Arcaro MJ, Pinsk MA, & Kastner S (2015b). The anatomical and functional organization of the human visual pulvinar. Journal of Neuroscience, 35, 9848–9871. [PubMed: 26156987]

Arcelli P, Frassoni C, Regondi MC, Biasi SD, & Spreafico R (1997). GABAergic neurons in mammalian thalamus: A marker of thalamic complexity? Brain Research Bulletin, 42, 27–37. [PubMed: 8978932]

Arend I, Machado L, Ward R, McGrath M, Ro T, Rafal RD (2008). The role of the human pulvinar in visual attention and action: evidence from temporal-order judgment, saccade decision, and antisaccade tasks. Progress in Brain Research, 171, 475–483. [PubMed: 18718343]

Barron BS, Eickhoff SB, Clos M, & Fox PT (2015). Human pulvinar functional organization and connectivity. Human Brain Mapping, 36, 2417–2431. [PubMed: 25821061]

Baleydier C, & Mauguiere F (1985). Anatomical evidence for medial pulvinar connections with the posterior cingulate cortex, the retrosplenial area, and the posterior parahippocampal gyrus in monkeys. Journal of Comparative Neurology. 232, 219–228.

Behrens TEJ, Woolrich MW, Jenkinson M, Johansen-Berg H, Nunes RG, Clare S, Matthews PM, Brady JM, Smith SM (2003). Characterization and Propagation of Uncertainty in Diffusion-Weighted MR Imaging. Magnetic Resonance in Medicine, 50, 1077–1088. [PubMed: 14587019]

Behrens TEJ, Berg HJ, Jbabdi S, Rushworth MFS, & Woolrich MW (2007). Probabilistic diffusion tractography with multiple fibre orientations: What can we gain? Neuroimage, 34, 144–155. [PubMed: 17070705]

Bickford ME, Wei H, Eisenback MA, Chomsung RD, Slusarczyk AS, Dankowsi AB (2008). Synaptic organization of thalamocortical axon collaterals in the perigeniculate nucleus and dorsal lateral geniculate nucleus. Journal of a Comparative Neurology, 508, 264–285.

Bowery NG, Hudson AL, & Price GW (1987). $GABA_A$ and $GABA_B$ receptor site distribution in the rat central nervous system. Neuroscience, 20, 365–383. [PubMed: 3035421]

Bowery NG, Parry K, Goodrich G, Ilinsky I, & Kultas-Ilinsky K (1999). Distribution of GABA(B) binding sites in the thalamus and basal ganglia of the rhesus monkey (Macaca mulatta). Neuropharmacology, 38, 1675–1682. [PubMed: 10587083]

Buschman TJ, & Kastner S (2015). From behavior to neural dynamics: An integrated theory of attention. Neuron, 88, 127–144. [PubMed: 26447577]

Buzsákil G, & Wang XJ (2012). Mechanisms of Gamma Oscillations. Annual Review of Neuroscience, 35, 203–225.

Cardin JA, Carlén M, Meletis K, Knoblich U, Zhang F, Deisseroth K, Tsai L-H, & Moore CI (2009). Driving fast-spiking cells induces gamma rhythm and controls sensory responses. Nature, 459, 663–667. [PubMed: 19396156]

Crabtree JW (2018). Functional Diversity of Thalamic Reticular Subnetworks. Frontiers in Systems Neuroscience, 12, 1–41. [PubMed: 29434540]

Desimone R, Wessinger M, Thomas L, & Schneider W (1990). Attentional control of visual perception: cortical and subcortical mechanisms. Cold Spring Harbor symposia on quantitative biology, 55, 963–971. [PubMed: 2132873]

Fiebelkorn IC, Pinsk MA, & Kastner S (2019a). The mediodorsal pulvinar coordinates the macaque fronto-parietal network during rhythmic spatial attention. Nature Communication, 10, 215.

Fiebelkorn IC, & Kastner S (2019b). A Rhythmic Theory of Attention. Trends Cogn. Sci. 23, 87–101. [PubMed: 30591373]

Fiebelkorn IC, & Kastner S (2020). Functional Specialization in the Attention Network. Annual Review of Psychology, 71, 221–249.

Friedman-Hill SR, Robertson LC, Desimone R, & Ungerleider LG (2003). Posterior parietal cortex and the filtering of distractors. Proceedings of National Academy of Sciences U. S. A, 100, 4263–4268.

Fries P, Reynolds JH, Rorie AE, & Desimone R (2001). Modulation of oscillatory neuronal synchronization by selective visual attention. Science, 291, 1560–1563. [PubMed: 11222864]

Gattass R, Galkin TW, Desimone R, & Ungerleider LG (2014). Subcortical connections of area V4 in the macaque. Journal of Comparative Neurology, 522, 1941–1965.

Gutierrez C, Cola MG, Seltzer B, & Cusick C (2000). Neurochemical and connectional organization of the dorsal pulvinar complex in monkeys. Journal ofa Comparative Neurology, 419, 61–86.

Halassa MM, & Kastner S (2017). Thalamic functions in distributed cognitive control. Nature Neuroscience, 20, 1669–1679. [PubMed: 29184210]

Halassa MM, Chen Z, Wimmer RD, Brunetti PM, Zhao S, Zikopoulos B, Wang F, Brown EN, & Wilson MA (2014). State-dependent architecture of thalamic reticular subnetworks. Cell, 158, 808–821. [PubMed: 25126786]

Han S, Jiang Y, Gu H, Rao H, Mao L, Cui Y, & Zhai R (2004). The role of human parietal cortex in attention networks. Brain, 127, 650–659. [PubMed: 14761902]

Hernández M, Guerrero GD, Cecilia JM, García JM, Inuggi A, Jbabdi S, Behrens TEJ, & Sotiropoulos SN (2013). Accelerating fibre orientation estimation from diffusion weighted magnetic resonance imaging using GPUs. PLoS One, 8, e61892. [PubMed: 23658616]

Huang X, Ye C-C, Zhong Y-L, Ye L, Yang Q-C, Li H-J, Jiang N, Peng D-C, & Shao Y. (2017). Altered regional homogeneity in patients with late monocular blindness: A resting-state functional MRI study. Neuroreport, 28, 1085–1091. [PubMed: 28858036]

Hughes SW, & Crunelli V (2005). Thalamic Mechanisms of EEG Alpha Rhythms and Their Pathological Implications. The Neuroscientist, 11, 357–372. [PubMed: 16061522]

Hughes SW, Lorincz M, Cope DW, Blethyn KL, Kekesi KA, Parri HR, Juhasz G, & Crunelli V (2004). Synchronized Oscillations at θ and α Frequencies in the Lateral Geniculate Nucleus. Neuron, 42, 253–268. [PubMed: 15091341]

Hunt CA, Pang DZ, & Jones EG (1991). Distribution and density of GABA cells in intralaminar and adjacent nuclei of monkey thalamus. Neuroscience, 43, 185–196. [PubMed: 1922765]

Huntsman MM, Leggio MG, & Jones EG (1996). Nucleus-specific expression of $GABA_A$ receptor subunit mRNAs in monkey thalamus. Journal of Neuroscience, 16, 3571–3589. [PubMed: 8642403]

Jaramillo J, Mejias JF, & Wang XJ (2019). Engagement of Pulvino-cortical Feedforward and Feedback Pathways in Cognitive Computations. Neuron, 101, 321–336. [PubMed: 30553546]

Jbabdi S, Sotiropoulos SN, Savio AM, Graña M, & Behrens TEJ (2012). Model-based analysis of multishell diffusion MR data for tractography: How to get over fitting problems. Magnetic Resonance in Medicine, 68, 1846–1855. [PubMed: 22334356]

John YJ, Zikopoulos B, Bullock D, & Barbas H (2018). Visual Attention Deficits in Schizophrenia Can Arise From Inhibitory Dysfunction in Thalamus or Cortex. Computational Psychiatry, 2, 1–35. [PubMed: 30090859]

Kaas JH, & Lyon DC (2007). Pulvinar contributions to the dorsal and ventral streams of visual processing in primates. Brain Research Review, 55, 285–296.

Kastner S, & Ungerleider LG (2000). Mechanisms of visual attention in the human cortex. Annual Reviews in Neuroscience, 23, 315–341.

Kastner S, Fiebelkorn IC, & Eradath MK (2020). Dynamic pulvino-cortical interactions in the primate attention network. Current Opinion in Neurobiology, 65, 10–19. [PubMed: 32942125]

Kellner E, Dhital B, Kiselev VG, & Reisert M (2016). Gibbs-Ringing Artifact Removal Based on Local Subvoxel-Shifts. Magnetic Resonance in Medicine, 76, 1574–1581. [PubMed: 26745823]

Lachaux JP, Rodriguez E, Martinerie J & Varela FJ (1999). Measuring phase synchrony in brain signals. Human Brain Mapping, 8, 194–208. [PubMed: 10619414]

Lorincz ML, Cranelli V, & Hughes SW (2008). Cellular Dynamics of Cholinergically Induced α (8 –13 Hz) Rhythms in Sensory Thalamic Nuclei *In Vitro*. Journal of Neuroscience, 28, 660–671. [PubMed: 18199766]

Majchrzak M, & Di Scala G (2000). GABA and muscimol as reversible inactivation tools in learning and memory. Neural Plasticity, 7, 19–29. [PubMed: 10709211]

Mantini D, Corbetta M, Romani GL, Orban GA, & Vanduffel W (2013). Evolutionarily novel functional networks in the human brain? Journal of Neuroscience, 33, 3259–3275. [PubMed: 23426655]

McAlonan K, Cavanaugh J, & Wurtz RH (2008). Guarding the gateway to cortex with attention in visual thalamus. Nature, 456, 391–394. [PubMed: 18849967]

Mccormick DA, & Prince DA (1987). Neurotransmitter Modulation of Thalamic Neuronal Firing Pattern. The Journal of Mind and Behavior, 8, 573–590.

Moeller S, Nallasamy N, Tsao DY, & Freiwald WA (2009). Functional connectivity of the macaque brain across stimulus and arousal states. Journal of Neuroscience, 29, 5897–5909. [PubMed: 19420256]

Neto FL, Ferreira-Gomes J, & Castro-Lopes JM (2006). Distribution of GABA Receptors in the Thalamus and Their Involvement in Nociception. Advances in Pharmacology, 54, 29–51. [PubMed: 17175809]

Park A, Hoffman K, & Keller A (2014). Roles of $GABA_A$ and $GABA_B$ receptors in regulating thalamic activity by the zona incerta: a computational study. Journal of Neurophysiol, 112, 2580–2596.

Perrone D, Aelterman J, Pižurica A, Jeurissen B, Philips W, & Leemans A (2015). The effect of Gibbs ringing artifacts on measures derived from diffusion MRI. NeuroImage, 120, 441–455. [PubMed: 26142273]

Pesaran B (2010). Neural correlations, decisions, and actions. Current Opinion in Neurobiology, 20, 166–171. [PubMed: 20359885]

Petersen SE, Robinson DL, & Morris JD (1987). Contributions of the pulvinar to visual spatial attention. Neuropsychologia, 25, 97–105. [PubMed: 3574654]

Pinault D (2004). The thalamic reticular nucleus: structure, function and concept. Brain Research Brain Research Reviews, 46, 1–31. [PubMed: 15297152]

Posner MI, Walker JA, Friedrich FJ, & Rafal RD (1984). Effects of parietal injury on covert orienting of attention. Journal of Neuroscience, 4, 1863–1874. [PubMed: 6737043]

Purushothaman G, Marion R, Li K, & Casagrande VA (2012). Gating and control of primary visual cortex by pulvinar. Nature Neuroscience, 15, 905–912. [PubMed: 22561455]

Rafal RD, & Posner MI (1987). Deficits in human visual spatial attention following thalamic lesions. Proceedings of National Academy of Sciences U. S. A, 84, 7349–53.

Ray S, & Maunsell JHR (2011). Different origins of gamma rhythm and high-gamma activity in macaque visual cortex. PLoS Biol. 9.

Ray S, Crone NE, Niebur E, Franaszczuk PJ, & Hsiao SS (2008). Neural correlates of high-gamma oscillations (60-200 Hz) in macaque local field potentials and their potential implications in electrocorticography. Journal of Neuroscience, 28, 11526–11536. [PubMed: 18987189]

Reveley C, Gruslys A, Ye FQ, Glen D, Samaha J, Russ BE, Saad Z, Seth AK, Leopold DA, & Saleem KS (2017). Three-Dimensional Digital Template Atlas of the Macaque Brain. Cerebral Cortex, 27, 4463–4477. [PubMed: 27566980]

Robinson DL, & Petersen SE (1992). The pulvinar and visual salience. Trends in Neuroscience, 15, 127–132.

Saalmann YB, & Kastner S (2011). Cognitive and Perceptual Functions of the Visual Thalamus. Neuron, 71, 209–223. [PubMed: 21791281]

Saalmann YB, Ly R, Pinsk MA, & Kastner S (2018). Pulvinar influences parietal delay activity and information transmission between dorsal and ventral visual cortex in macaques. Biorxiv.

Saalmann YB, Pinsk MA, Wang L, Li X, & Kastner S (2012). Pulvinar regulates information transmission between cortical areas based on attention demands. Science, 337, 753–756. [PubMed: 22879517]

Saleem KS, & Logothetis NK (2007). A combined MRI and histology atlas of the rhesus monkey brain in stereotaxic coordinates. 2nd ***ed*** San Diego: Elsevier/Academic press.

Sherman SM (2007). The thalamus is more than just a relay. Current Opinion in Neurobiology, 17, 417–422. [PubMed: 17707635]

Shipp S (2001). Corticopulvinar Connections of Areas V5, V4 , and V3 in the Macaque Monkey : A Dual Model of Retinal and Cortical Topographies. Journal of Comparative Neurology, 490, 469–490.

Shipp S (2003). The functional logic of cortico-pulvinar connections. Philosophical transactions of the Royal Society of London. Series B, Biological sciences, 358, 1605–1624. [PubMed: 14561322]

Silva LR, Amitai Y, & Connors BW (1991). Intrinsic oscillations of neocortex generated by layer 5 pyramidal neurons. Science, 251, 432–435. [PubMed: 1824881]

Sivilotti L, & Nistri A (1991). GABA receptor mechanisms in the central nervous system. Progress in Neurobiology, 36, 35–92. [PubMed: 1847747]

Snow JC, Allen HA, Rafal RD, & Humphreys GW (2009). Impaired attentional selection following lesions to human pulvinar: Evidence for homology between human and monkey. Proceedings in National Academy of Sciences U. S. A, 106, 4054–4059.

Stein T, Moritz C, Quigley M, Cordes D, Haughton V, & Meyerand E (2000). Functional connectivity in the thalamus and hippocampus studied with functional MR imaging. American Journal of Neuroradiology, 21, 1397–1401. [PubMed: 11003270]

Steriade M, Domich L, Oakson G, & Deschenes M (1987). The deafferented reticular thalamic nucleus generates spindle rhythmicity. Journal of Neurophysiology, 57, 260–273. [PubMed: 3559675]

Terpou BA, Densmore M, Théberge J, Frewen P, McKinnon MC, & Lanius RA (2018). Resting-state pulvinar-posterior parietal decoupling in PTSD and its dissociative subtype. Human Brain Mapping, 39, 4228–4240. [PubMed: 30091811]

Theyel BB, Llano DA, & Sherman SM (2010). The corticothalamocortical circuit drives higher-order cortex in the mouse. Nature Neuroscience, 13, 84–88. [PubMed: 19966840]

Tremblay R, Lee S, & Rudy B (2016). GABAergic interneurons in the neocortex: From cellular properties to circuits. Neuron, 91, 260–292. [PubMed: 27477017]

Trojanowski JQ, & Jacobson S (1974). Medial pulvinar afferents to frontal eye fields in rhesus monkey demonstrated by horseradish peroxidase. Brain Research, 80, 395–411. [PubMed: 4138113]

Tournier JD, Smith R, Raffelt D, Tabbara R, Dhollander T, Pietsch M, Christiaens D, Jeurissen B, Yeh CH, Connelly A (2019). MRtrix3: A fast, flexible and open software framework for medical image processing and visualization. NeuroImage, 202.

Vanderwal T, Eilbott J, & Castellanos FX (2019). Movies in the magnet: Naturalistic paradigms in developmental functional neuroimaging. Developmental cognitive neuroscience, 36, 100600. [PubMed: 30551970]

Vanderwal T, Kelly C, Eilbott J, Mayes LC, & Castellanos FX (2015). Inscapes: a movie paradigm to improve compliance in functional magnetic resonance imaging. Neuroimage, 122, 222–232. [PubMed: 26241683]

Veraart J, Novikov DS, Christianens D, Ades-aron B, Sijbers J, & Fieremanns E (2016). Denoising of diffusion MRI using random matrix theory. Neuroimage, 142, 394–406. [PubMed: 27523449]

Vijayan S, & Kopell NJ (2012). Thalamic model of awake alpha oscillations and implications for stimulus processing. Proceedings of National Academy of Sciences, 109, 18553–18558.

Vinck M, Wingerden M, Womelsdorf T, Fries P, Pennartz CMA (2010). The pairwise phase consistency: A bias-free measure of rhythmic neuronal synchronization. NeuroImage, 51, 112–122. [PubMed: 20114076]

Wang L, Saalmaan Y, Pinsk MA, Arcaro MJ, & Kastner S (2012). Electrophysiological low-frequency coherence and frequency coupling contributes to BOLD connectivity. Neuron 76, 1010–1020. [PubMed: 23217748]

Ward R, Danziger S, Owen V, & Rafal R (2002). Deficits in spatial coding and feature binding following damage to spatiotopic maps in the human pulvinar. Nature Neuroscience, 5, 99–100. [PubMed: 11780145]

Watson RT, Heilman KM, Cauthen JC, & King FA (1973). Neglect after cingulectomy. Neurology, 23, 1003–1007. [PubMed: 4199186]

Watson BO, Ding M, & Buzsáki G (2018). Temporal coupling of field potentials and action potentials in the neocortex. European Journal of Neuroscience, 48, 2482–2497.

Whittington MA, Traub RD, Kopell N, Ermentrout B, Buhl EH (2000). Inhibition-based rhythms: experimental and mathematical observations on network dynamics. International Journal of Psychophysiology, 38, 315–336. [PubMed: 11102670]

Wilke M, Mueller KM, & Leopold DA (2009). Neural activity in the visual thalamus reflects perceptual suppression. Proceedings of National Academy of Sciences U S A., 106, 9465–9470.

Wilke M, Turchi J, Smith K, Mishkin M, & Leopold DA (2010). Pulvinar Inactivation Disrupts Selection of Movement Plans. Journal of Neuroscience, 30, 8650–8659. [PubMed: 20573910]

Wimmer RD, Schmitt LI, Davidson TJ, Nakajima M, Deisseroth K, & Halassa MM (2015). Thalamic control of sensory selection in divided attention. Nature, 526, 705–709. [PubMed: 26503050]

Yeterian EH, & Pandya DN (1985). Corticothalamic connections of the posterior parietal cortex in the rhesus monkey. Journal of Comparative Neurology, 237, 408–426.

Zhou H, Schafer RJ, & Desimone R (2016). Pulvinar-Cortex interactions in vision and attention. Neuron, 89, 209–220. [PubMed: 26748092]

Zikopoulos B, & Barbas H (2007). Circuits for multisensory integration and attentional modulation through the prefrontal cortex and the thalamic reticular nucleus in primates. Reviews in the Neurosciences, 18, 417–438. [PubMed: 18330211]

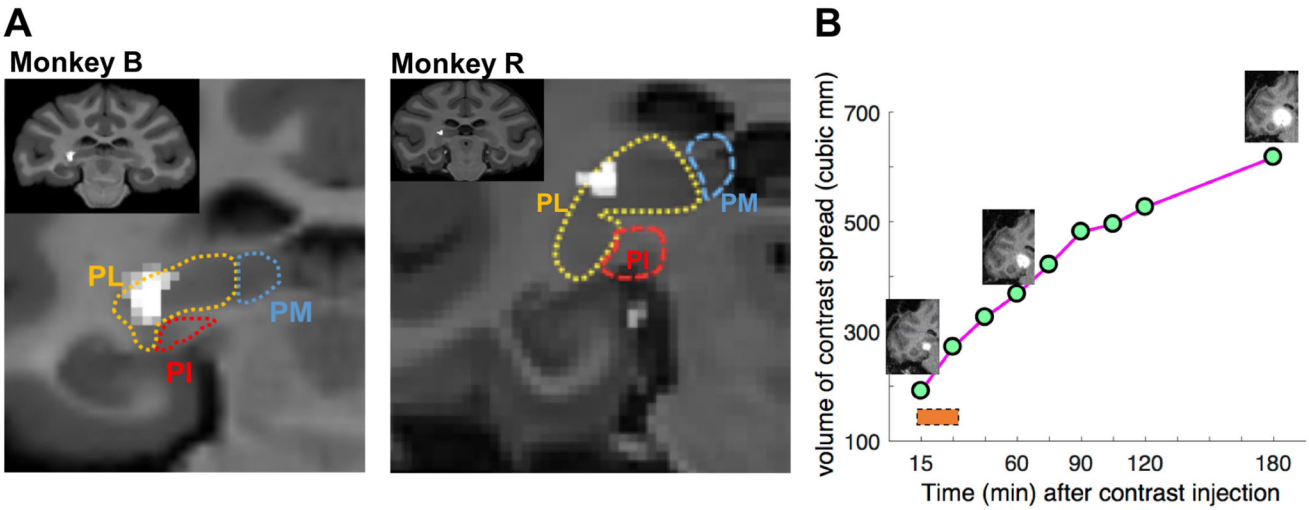

Figure 1. Anatomical localization of inactivation zone.

(A) Structural MRI scan visualizing the initial site of a Gadolinium MRI contrast agent injection (0.5μl) in monkey B and monkey R. MR images of individual animals were non-linearly wrapped onto the D99 digital template atlas to approximate the boundaries of pulvinar subdivisions. PM: Medial pulvinar, PL: Lateral pulvinar, PI: Inferior pulvinar. The injection site was localized within dorsal portions of the lateral pulvinar (dPL) for both monkeys. (B) Serial MRI images showing the spread of Gadolinium contrast agent over a duration of 3 hours, following injection into dPL. The inserts visualize the spread of the contrast agent at 15, 60, and 180 minutes, respectively, after the end of the contrast injection, during one session in monkey B. The orange bar indicates the time window (15-minutes, starting from 15 minutes after the end of injection) used for the post-injection analyses of recordings.

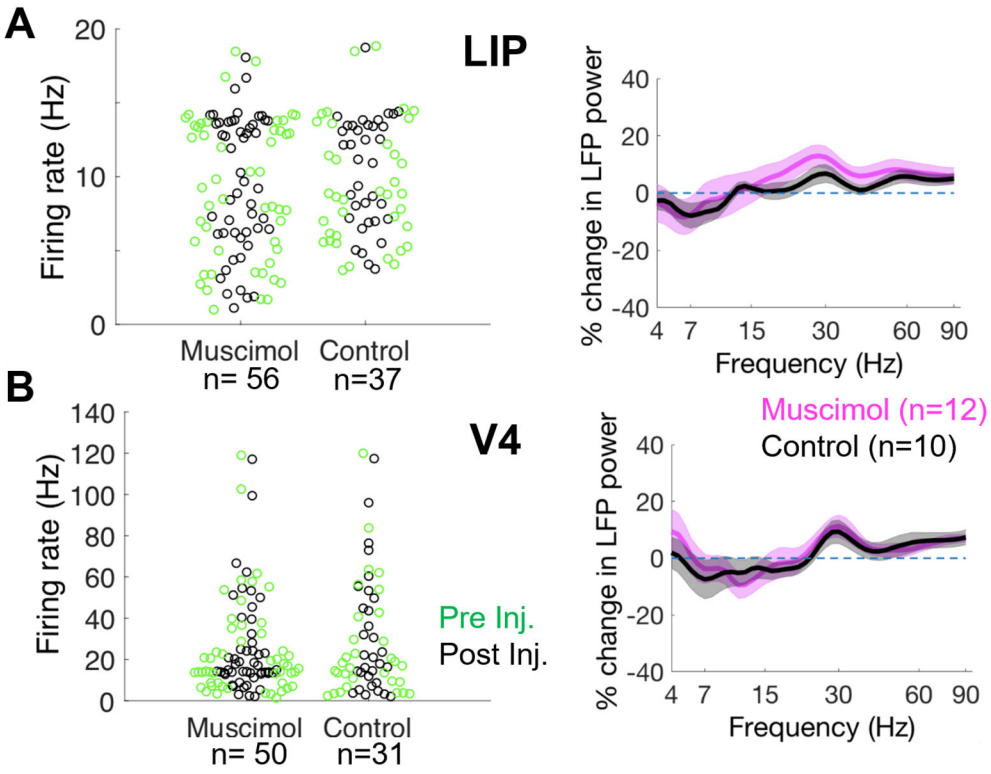

Figure 2. dPL inactivation did not significantly change spike rates and local field potential power in LIP and V4.

(A) Left: Changes in LIP spike rates before (green) and after (black) muscimol or control injections into dPL. Right: Percentage change in local field potential (LFP) power in LIP across a frequency range of 4-90 Hz during post vs. pre-injection windows, for muscimol (magenta) and saline control (black) injections. (B) Left: Changes in V4 spike rates before (green) and after (black) muscimol or control injections into dPL. Right: Percentage change in local field potential (LFP) power of V4 across a frequency range of 4-90 Hz during post vs. pre-injection windows, for muscimol (magenta) and saline control (black) injections. Combined data from both monkeys. (Error bars/shaded areas: s.e.m.).

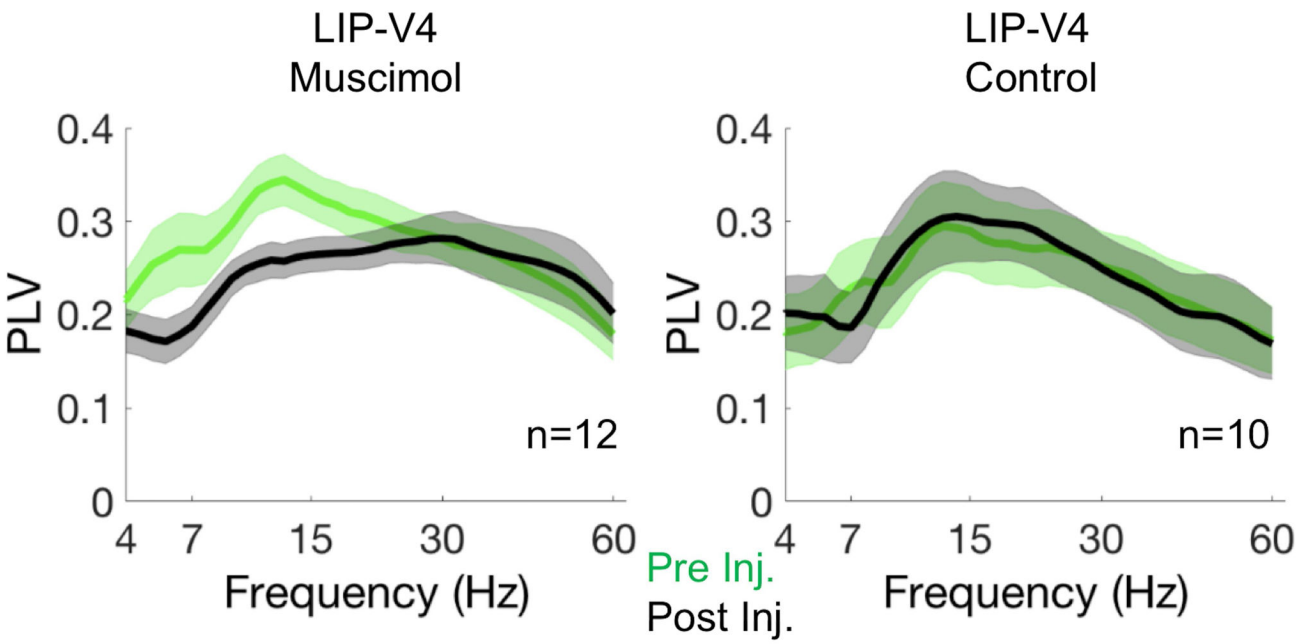

Figure 3. LFP-LFP coherence between LIP and V4 significantly decreased following pulvinar inactivation.

Strength of LFP-LFP phase coherence (measured as phase locking value – PLV) between LIP and V4 across a 4-60 Hz frequency range during pre- (green) and post- (black) injection windows, shown separately for muscimol (left) and control (right) sessions. The post-injection LFP-LFP phase coherence between LIP and V4 was significantly lower compared to the pre-injection coherence in theta (4-7 Hz) and alpha/low beta (7-15 Hz) frequency ranges for muscimol, but not for control sessions. Combined data from both monkeys. Shaded areas: s.e.m..

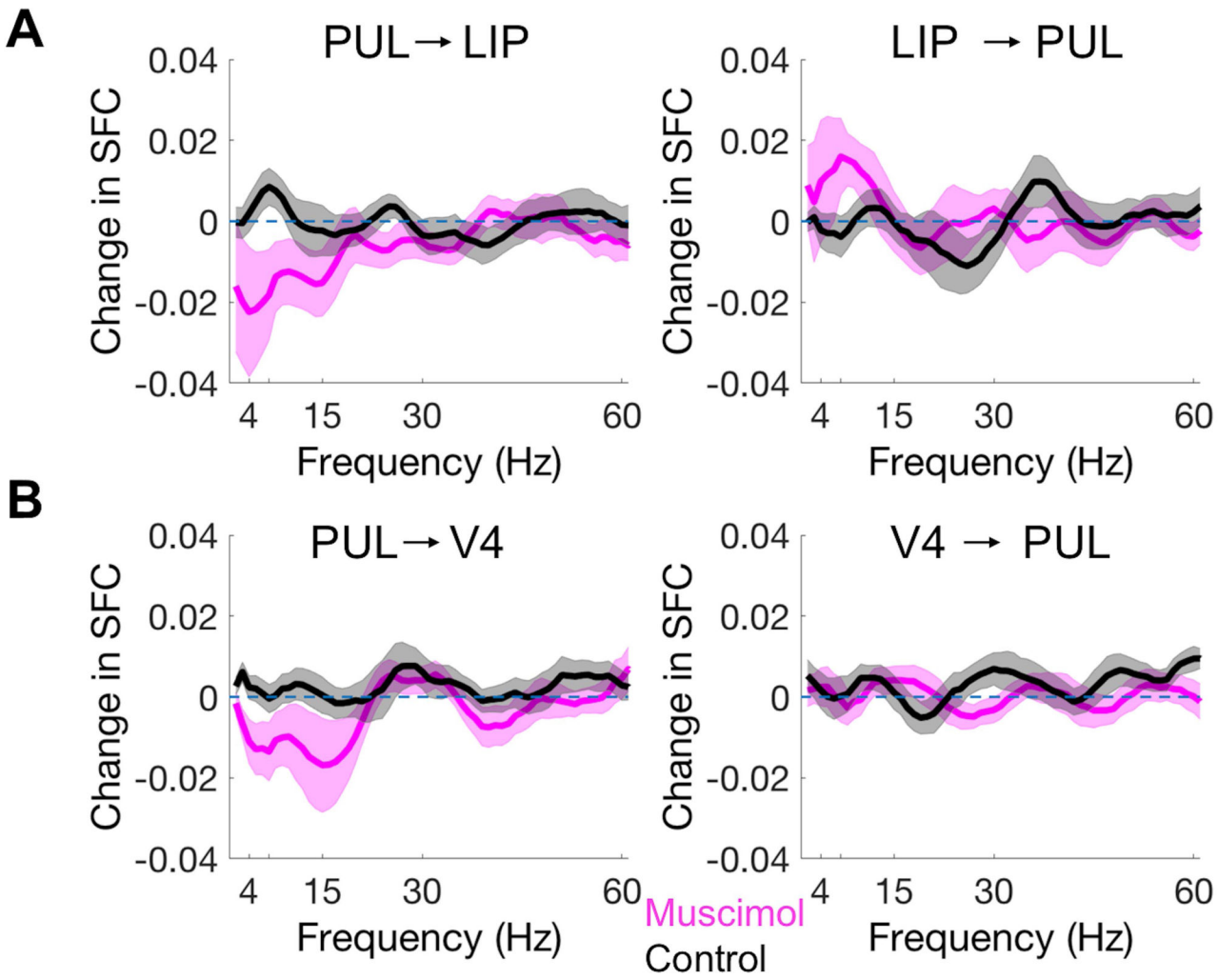

Figure 4. Changes in spike-field coherence (SFC) between pulvinar and cortical areas following dPL injections.

(A) Left: Change in SFC between pulvinar spikes and LIP LFP phase over a frequency range of 4-60 Hz during post vs. pre-injection windows for muscimol (magenta) and control (black) sessions. The dPL spike-LIP phase coherence decreased significantly in the 4-15 Hz range following muscimol injections into dPL. Right: Change in SFC between LIP spikes and pulvinar LFP phase during post vs. pre-injection windows for muscimol (magenta) and control (black) sessions. The LIP spike-pulvinar phase coherence increased significantly in the 4-15 Hz range following muscimol injections. (B) Left: change in SFC between pulvinar spikes and V4 LFP phase during post vs. pre-injection windows for muscimol (magenta) and control (black) sessions. The dPL spike-V4 phase coherence decreased significantly in the 4-15 Hz range following muscimol injections into dPL. Right: Change in SFC between V4 spike and pulvinar LFP phase during post vs. pre-injection windows for muscimol (magenta) and control (black) sessions. Shaded areas: s.e.m..

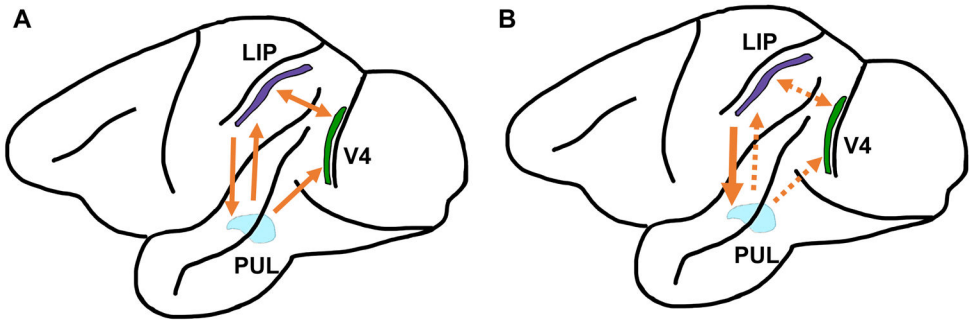

Figure 5. Thalamo-cortical interactions under normal conditions (A) and during pulvinar inactivation (B).

Typically, pulvinar influences cortical regions (here LIP and V4) to coordinate cortico-cortical interactions (A). After muscimol injections into dPL, pulvinar influences on LFP phase of LIP and V4 decreased significantly in low frequencies (4 - 15 Hz). At the same time, low frequency coherence from LIP, but not V4, to pulvinar significantly increased following dPL inactivation, suggesting that the transthalamic pathway is under parietal cortex control (B).